Monthly Notices
of the
ROYAL ASTRONOMICAL SOCIETY

MNRAS **436,** 3557–3572 (2013) doi:10.1093/mnras/stt1834
Advance Access publication 2013 October 24

The High Time Resolution Universe survey – IX. Polarimetry of long-period pulsars

C. Tiburzi,[1,2]⋆ S. Johnston,[3] M. Bailes,[4,5] S. D. Bates,[6] N. D. R. Bhat,[5,7] M. Burgay,[1] S. Burke-Spolaor,[8] D. Champion,[9] P. Coster,[3,4] N. D'Amico,[1,2] M. J. Keith,[10] M. Kramer,[9,10] L. Levin,[6] S. Milia,[1] C. Ng,[9] A. Possenti,[1] B. W. Stappers,[10] D. Thornton[3,10] and W. van Straten[4,5]

[1]*INAF – Osservatorio Astronomico di Cagliari, Via della Scienza, I-09047 Selargius (CA), Italy*
[2]*Dipartimento di Fisica, Università di Cagliari, Cittadella Universitaria, I-09042 Monserrato (CA), Italy*
[3]*CSIRO Astronomy & Space Science, Australia Telescope National Facility, PO Box 76, Epping, NSW 1710, Australia*
[4]*Centre for Astrophysics and Supercomputing, Swinburne University of Technology, Mail H39, PO Box 218, VIC 3122, Australia*
[5]*ARC Centre of Excellence for All-sky Astrophysics, 44 Rosehill Street Redfern, NSW 2016, Australia*
[6]*Department of Physics, West Virginia University, Morgantown, WV 26506, USA*
[7]*International Centre for Radio Astronomy Research, Curtin University, Bentley, WA 6102, Australia*
[8]*Jet Propulsion Laboratory, California Institute of Technology, 4800 Oak Grove Drive, Pasadena CA 91104, USA*
[9]*Max Planck Institut für Radioastronomie, Auf dem Hügel 69, D-53121 Bonn, Germany*
[10]*Jodrell Bank Centre for Astrophysics, University of Manchester, Alan Turing Building, Oxford Road, Manchester M13 9PL, UK*

Accepted 2013 September 26. Received 2013 September 24; in original form 2013 May 20

ABSTRACT

We present a polarimetric analysis of 49 long-period pulsars discovered as part of the High Time Resolution Universe (HTRU) southern survey. The sources exhibit the typical characteristics of 'old' pulsars, with low fractional linear and circular polarization and narrow, multi-component profiles. Although the position angle swings are generally complex, for two of the analysed pulsars (J1622−3751 and J1710−2616) we obtained an indication of the geometry via the rotating vector model. We were able to determine a value of the rotation measure (RM) for 34 of the sources which, when combined with their dispersion measures (DM), yields an integrated magnetic field strength along the line of sight. With the data presented here, the total number of values of RM associated with pulsars discovered during the HTRU southern survey sums to 51. The RMs are not consistent with the hypothesis of a counter-clockwise direction of the Galactic magnetic field within an annulus included between 4 and 6 kpc from the Galactic Centre. A partial agreement with a counter-clockwise sense of the Galactic magnetic field within the spiral arms is, however, found in the area of the Carina-Sagittarius arm.

Key words: magnetic fields – polarization – methods: observational – pulsars: general.

1 INTRODUCTION

Pulsars are rapidly rotating neutron stars, characterized by an extremely intense magnetic field, whose first-order term is a dipole. They are in general broad-band emitters powered by their spin-down energy. In particular, at radio wavelengths they are observed to be faint pulsating sources: two emission beams are generated from the magnetic poles due to streams of charged particles that are accelerated along the magnetic field lines. Assuming a misalignment between the rotational and the magnetic axes, the two radiation beams sweep across the sky. If the observer's line of sight crosses one or both of them, pulsations can be observed. Although this model is well supported by observations, many details are still not completely understood, e.g. the exact structure of the beams, their time evolution and how the emitting regions are distributed within the beams.

One method used for determining the geometry of the star and the beam structure is polarization analysis. The radio emission from pulsars is among the most polarized we receive from celestial objects, showing an average degree of linear polarization L up to 20 per cent in the sources with a spin-down luminosity ($\dot{E}$) less than 5×10^{33} erg s^{-1} and exceeding 50 per cent in those where $\dot{E} > 2 \times 10^{35}$ erg s^{-1} (see Gould & Lyne 1998; von Hoensbroech, Lesch & Kunzl 1998; Weltevrede & Johnston 2008). Unlike the degree of circular polarization (smaller but still significant, around 10 per cent), L is typically anti-correlated with observing frequency (e.g. Johnston et al. 2008).

In the 'rotating vector model' (RVM; Radhakrishnan & Cooke 1969), the linear polarization orientation [observed as the position

⋆ E-mail: ctiburzi@oa-cagliari.inaf.it

angle (PA)] is determined by the orientation of the magnetic field lines. While observing a pulse, the line of sight crosses the magnetic field lines with a continuously changing orientation. Hence, an S-shaped swing in the PA value is expected. The RVM provides the formalism, whereby the swing shape is determined by the pulsar's geometric parameters (the impact parameter between the line of sight and the magnetic axis and the misalignment between the spin and the magnetic axes, the angle α). In turn then, the knowledge of the PA swing can, in principle, allow a determination of the geometry (see e.g. Everett & Weisberg 2001). Moreover, from the delay in longitude between the PA swing and the total power peak due to retardation and aberration effects (Blaskiewicz, Cordes & Wasserman 1991; Hibschman & Arons 2001; Gupta & Gangadhara 2003), it is possible to infer the emission altitude (von Hoensbroech & Xilouris 1997; Johnston & Weisberg 2006). However, it is rare that the RVM can be applied: often the narrow longitude pulse window prevents a unique determination of the geometry. Besides this, many 'forbidden' PA profiles are observed, e.g. characterized by flat trends or complex variations in the PA profile as abrupt jumps of about $\sim 90^{\circ}$. This has been explained (Backer, Rankin & Campbell 1976; Cordes, Rankin & Backer 1978) with the presence of two orthogonal polarization modes (OPM; McKinnon & Stinebring 2000) in pulsar emissions. The changes in the relative amplitude between the two modes induce sudden variations in the PA profile. Several cases of non-orthogonal PA jumps have also been reported (Karastergiou, Johnston & Manchester 2005). The occurrence of OPM (and also non-orthogonal) PA jumps induces a linear depolarization, due to the incoherent mix of the modes. In particular, old pulsars and millisecond pulsars often display complicated PA profiles that are inconsistent with the RVM predictions [see e.g. Johnston & Weisberg (2006), Johnston et al. (2008), Xilouris et al. (1998), Stairs, Thorsett & Camilo (1999), Yan et al. (2011)].

Circular polarization is usually brighter in the centre (or core) of a pulse profile (Rankin 1993; Gould & Lyne 1998). It often shows handedness variability as a function of the pulse longitude (Radhakrishnan & Rankin 1990), and in many cases hand reversal also occurs near the profile centre. This gives a further hint about the location of the magnetic axis, and a possible relationship between the PA swing sense and the handedness of the circular polarization is debated (Han et al. 1998). A more reliable connection appears to be between the circularly polarized emission and the OPM jumps. In fact, Karastergiou & Johnston (2004) showed that a strong correlation occurs between the presence of PA jumps and the variation in the handedness of the circular polarization. In spite of the complex nature of pulsar polarization, polarimetry of pulsars gives a unique insight into the three-dimensional structure of the beam above the polar caps (Rankin 1983; Lyne & Manchester 1988; Han & Manchester 2001; Karastergiou & Johnston 2007; Beskin & Philippov 2012).

Another use of polarization analysis is in probing the magnetic field structure of the medium crossed by the radiation. A polarized signal that propagates through an ionized and magnetized medium (see Section 3) undergoes differential propagation velocity between its (right- and left-handed) components. This effect, known as the Faraday rotation, that is a birefringence phenomenon, induces a rotation in the PA. This is quantified through the rotation measure (RM) parameter, which depends on the ionized medium density and the magnetic field component along the line of sight. For pulsars, the polarized signal passes across three different kinds of ionized and magnetized medium: the pulsar magnetosphere, the Milky Way interstellar medium and Earth ionosphere. In pulsars, we can also quantify the average density of the ionized medium along the line of sight via the dispersion measure (DM) parameter and a combination of the RM and DM allows a direct measurement of the magnetic field along the line of sight.

Several attempts have been made to apply pulsar polarization analysis to probe the Galactic magnetic field structure (Manchester 1972; Manchester & Taylor 1977; Thomson & Nelson 1980; Lyne & Smith 1989; Weisberg et al. 2004). In particular, the results obtained by Han & Qiao (1994), Han, Manchester & Qiao (1999), Han et al. (2002), Han et al. (2006) and Noutsos et al. (2008) suggest that the large scale in the magnetic field structure of the Milky Way disc is compatible with a bi-symmetric spiral, where the magnetic field in the spiral arms is mainly counter-clockwise if seen from the Galactic north, and the field in between the arms is chiefly clockwise (Sofue & Fujimoto 1983). On the other hand, the work of Vallée (2005) supports a general clockwise orientation of the large-scale Galactic magnetic field, with the presence of a counter-clockwise annulus included between 4 and 6 kpc from the Galactic Centre. It is clearly necessary to increase the RM sample in order to discriminate among the various hypotheses, and to guard against interstellar medium fluctuations and local turbulence in the magnetic field that could bias the RM estimation. An additional complication in this framework is RM fluctuation as a function of the pulse longitude. In particular, three sources of additional PA rotation beyond the large-scale Galactic magnetic field have been identified (Li & Han 2003; Ramachandran et al. 2004; Karastergiou 2009; Noutsos et al. 2009): the incoherent superposition of quasi-orthogonal polarization modes, the pulsar magnetosphere and scattering in the interstellar medium. In particular the latter is indicated as the most probable reason for the detected fluctuations.

The southern component of the High Time Resolution Universe survey for pulsars and fast transients (HTRU; Keith et al. 2010) is being carried out at the 64-m Parkes radio telescope. It is divided into three parts with different integration times depending on the Galactic latitude: low, medium and high. Since its beginning, it has led to the discovery of more than 100 pulsars. Among them there is a remarkable sample of millisecond pulsars (Bates et al. 2011; Keith et al. 2012; Burgay et al. 2013, Thornton et al., in preparation; Ng et al., in preparation). However, the majority of them are normal pulsars (Bates et al. 2012; Ng et al., in preparation). Following the presentation of the millisecond pulsar polarimetry (Keith et al. 2012; Burgay et al. 2013), in this work we present a systematic polarization analysis of 48 long-period pulsars discovered in the medium latitude part of the survey, and one discovered in the high latitude part.

2 OBSERVATIONS AND ANALYSIS

We present the polarization analysis of a sample of 49 long-period pulsars, whose spin periods range from a few hundred milliseconds to about two and a half seconds. They were all discovered during the mid-latitude part of the HTRU survey (Keith et al. 2010; Bates et al. 2012) apart from PSR J1846−4249 (that has been discovered in the high latitude survey and it will be presented in one of the next papers of the HTRU series). PSR J1237−6725 and PSR J1539−4835 were originally thought to be new discoveries of the mid-latitude part of the HTRU survey but were first published by Kramer et al. (2003) and Eatough, Keane & Lyne (2009).

After discovery and confirmation, the pulsars were followed-up with the third Parkes Digital Filterbank, observing them for at least one year to allow the determination of a complete timing solution. The typical length of the timing observations ranges from ∼100 to ∼600 s. The data were acquired over a 256 MHz bandwidth centred

at 1369 MHz, split into 1024 frequency channels, each 0.25 MHz wide. The collected samples were folded on-line forming pulse profiles with 1024 bins for all four Stokes parameters in each frequency channel. To calibrate the target pointings for the differential gain and phase between the linear feeds, we made observations of noise diode coupled to the receptors in the feeds.

We reduced the data using the PSRCHIVE software package (Hotan, van Straten & Manchester 2004). For each individual observation, we first removed the radio frequency interference from the data. The observations were polarization-calibrated using a square wave signal in order to produce true Stokes parameters, and flux-calibrated using an averaged observation of Hydra A. In addition, corrections were made to the polarization impurity of the feed following the method in van Straten (2004). Finally, the observations were aligned using the best-fitting ephemeris and optimally summed weighting them according to the signal-to-noise ratio (SNR):

$$\mathrm{wt} = \frac{\mathrm{SNR}(I)}{\mathrm{rms}(I)} \tag{1}$$

where wt is the weight we applied and SNR(I) and rms(I) are the SNR and the off pulse root mean square of the total intensity profile, respectively.

This resulted in a higher SNR for the final profiles with respect to adding profiles based solely on the integration time. The resultant final profile still retained the full frequency information.

The next step was to compute the RM when possible. We collapsed the frequency channels to four, in order to enhance the SNR, and we computed an average PA across the bins of the pulse for each channel as in Noutsos et al. (2008):

$$PA_{\mathrm{ave}} = \frac{1}{2}\arctan\left(\frac{\sum_{i=n_{\mathrm{start}}}^{n_{\mathrm{end}}} U_i}{\sum_{i=n_{\mathrm{start}}}^{n_{\mathrm{end}}} Q_i}\right) \tag{2}$$

where Q_i and U_i are the Stokes parameters Q and U for the ith bin, and n_{start} and n_{end} are the bins of the pulse edges. In order to calculate the PA error bars we first measured the linear polarization as:

$$L_{\mathrm{meas}} = \sqrt{\left(\sum_{i=n_{\mathrm{start}}}^{n_{\mathrm{end}}} U_i\right)^2 + \left(\sum_{i=n_{\mathrm{start}}}^{n_{\mathrm{end}}} Q_i\right)^2}. \tag{3}$$

Since it is a positive definite quantity, the average value L_{meas} is biased. We followed the method of Wardle & Kronberg (1974) in order to obtain a better determination of the value of the linear polarization L_{true}:

$$L_{\mathrm{true}} = \begin{cases} 0.0 & \text{if } p_0 < 2.0 \\ \sqrt{L_{\mathrm{meas}}^2 - (\mathrm{rms}(I)\sqrt{n})^2} & \text{else} \end{cases} \tag{4}$$

where $p_0 = L_{\mathrm{meas}}/\mathrm{rms}(I)\sqrt{n_{\mathrm{pulse}}}$, where n_{pulse} is the on pulse number of bins.[1] Simmons & Stewart (1985) showed that this is the best method to be applied whenever p_0 is greater than 0.7 (see also Noutsos et al. 2008), as it happens in all the pulsars of our sample. As for the estimates of the uncertainties on $\mathrm{PA}_{\mathrm{ave}}$, $\sigma_{\mathrm{PA}_{\mathrm{ave}}}$, for high values ($P_0 > 10$) of $P_0 = L_{\mathrm{true}}/\mathrm{rms}(I)\sqrt{n_{\mathrm{pulse}}}$, we used the formula from Everett & Weisberg (2001):

$$\sigma_{\mathrm{PA}_{\mathrm{ave}}} = \frac{1}{2P_0}. \tag{5}$$

[1] For a handful of pulsars of our sample, we accepted a lower threshold for p_0 either in agreement with Everett & Weisberg (2001) or by visually inspecting that the PAs in the frequency channels where p_0 resulted less than 2 follow the trend predicted by equation (7).

For lower values of P_0, we numerically computed the error integrating the PA probability distribution between $\pm\sigma_{\mathrm{PA}_{\mathrm{ave}}}$ in order to obtain 0.68, as in Naghizadeh-Khouei & Clarke (1993) and Everett & Weisberg (2001):

$$G(\mathrm{PA} - \mathrm{PA}_{\mathrm{true}}; P_0) = \frac{1}{\sqrt{\pi}}\left\{\frac{1}{\sqrt{\pi}} + \eta_0 e^{\eta_0^2}[1 + \mathrm{erf}(\eta_0)]\right\} \times e^{-(P_0^2/2)} \tag{6}$$

where $\mathrm{PA}_{\mathrm{true}} = \mathrm{PA}_{\mathrm{ave}}$ in our case, $\eta_0 = (P_0\sqrt{2})\cos 2(\mathrm{PA} - \mathrm{PA}_{\mathrm{true}})$, erf is the Gaussian error function. We obtained the RM and its error implementing a least squares fit through the following equation:

$$\mathrm{PA}(f) = \mathrm{PA}_{\mathrm{ref}} + \mathrm{RM}c^2 \times \left(\frac{1}{f^2} - \frac{1}{f_{\mathrm{ref}}^2}\right) \tag{7}$$

where PA(f) is the PA at a certain frequency f, $\mathrm{PA}_{\mathrm{ref}}$ is the PA at a reference frequency f_{ref} and c is the speed of light. For pulsars with two recognizable components in the linear polarized profile, we fit for the RM separately for each component and we compared the obtained results *a posteriori*.

Once the RM was obtained, we summed over the frequency channels to produce the final integrated profile. A combination of low SNR and/or low polarization fraction meant that we were unable to compute the RM for a number of pulsars in our sample. In these cases, we simply set the RM to zero before summing over frequency.

A further useful quantity when considering pulsar polarization is the total amount of circular polarization irrespective of the handedness. The measured quantity $|V|_{\mathrm{meas}}$ is biased because it is positive definite. We followed Karastergiou & Johnston (2006) to obtain an unbiased value via:

$$|V|_{\mathrm{true}} = \begin{cases} 0.0 & \text{if } |V|_{\mathrm{meas}}/b < 2.0 \\ \sqrt{|V|_{\mathrm{meas}}^2 - b^2} & \text{else} \end{cases} \tag{8}$$

where

$$b = \sqrt{\frac{2}{\pi}} \times \mathrm{rms}(V). \tag{9}$$

Here, rms(V) is the root mean square of the off pulse V profile.

In order to quantify the luminosity and the percentage of polarization of the pulsars in our sample (showed in Tables 1 and 2), we computed the quantities S_0, L per cent, V per cent and $|V|$ per cent:

$$S_0 = \frac{1}{n_{\mathrm{bins}}}\sum_{i=n_{\mathrm{start}}}^{n_{\mathrm{end}}} I_i$$

$$L\ \text{per cent} = \frac{1}{n_{\mathrm{bins}}}\sum_{i=n_{\mathrm{start}}}^{n_{\mathrm{end}}} L_{\mathrm{true},i} \times \frac{100}{S_0}$$

$$V\ \text{per cent} = \frac{1}{n_{\mathrm{bins}}}\sum_{i=n_{\mathrm{start}}}^{n_{\mathrm{end}}} V_i \times \frac{100}{S_0}$$

$$|V|\ \text{per cent} = \frac{1}{n_{\mathrm{bins}}}\sum_{i=n_{\mathrm{start}}}^{n_{\mathrm{end}}} |V|_{\mathrm{true},i} \times \frac{100}{S_0} \tag{10}$$

where n_{bins} is the total number of phase bins that are present in the observations, $L_{i,\,\mathrm{true}}$, V_i and $|V|_{i,\,\mathrm{true}}$ are the (unbiased, in the cases of $L_{i,\,\mathrm{true}}$ and $|V|_{i,\,\mathrm{true}}$) values of linear, circular and absolute circular polarization in the ith phase bin. These definitions are consistent with those adopted by Gould & Lyne (1998).

Table 1. Pulsars for which RM can be determined. We show the spin period (P), the profile widths at 10 per cent (W_{10}) and 50 per cent (W_{50}) of the total intensity peak, the logarithm of the spin-down luminosity (Log $\dot{E}$), the total intensity flux ($S0$), the percentages of the linear, the circular and the absolute value of the circular polarisations (L per cent, V per cent, $|V|$ per cent), the rotation and the dispersion measures (RM and DM), the DM derived distance from the Sun (via the NE2001 electron density model from Cordes & Lazio 2002, that gives uncertainties up to about 30 per cent), the average value of the magnetic field along the line of sight ($< B_{||} >$) and the logarithm of the characteristic age (Log τ_C). 1σ errors on the last digit(s) are reported in parentheses. 3σ errors are reported for $S0$.

Name	P (s)	W_{10} (ms)	W_{50} (ms)	Log $\dot{E}$	S0 (mJy)	L per cent	V per cent	$\|V\|$ per cent	RM (rad m^{-2})	DM (pc cm^{-3})	Distance (kpc)	$< B_{\|\|} >$ (μG)	Log τ_C
J0807−5421	0.527	17	11	32.0	0.35(1)	14.5(7)	3(1)	5.8(6)	−65(3)	165	0.26	−0.48	7.3
J0905−6019	0.341	14	6	32.7	0.36(1)	5.8(7)	1(1)	1.3(7)	−63(23)	91	2.9	−0.85	7.0
J0912−3851	1.526	48	38	31.6	0.14(1)	22(1)	0(1)	10(1)	94(15)	63	0.5	1.85	6.8
J0949−6902	0.64	10	4	32.0	0.31(1)	6.5(8)	2(1)	3.6(7)	−58(14)	93	2.9	−0.77	7.2
J1036−6559	0.534	16	9	32.5	0.27(1)	12(1)	3(1)	5.2(9)	−88(20)	158	4.0	−0.69	6.8
J1105−4353	0.351	22	12	33.4	0.17(2)	23(2)	2(3)	4(2)	17(1)	38	1.4	0.56	6.3
J1237−6725	2.111	40	30	31.0	0.48(2)	4.8(9)	0(1)	1.6(8)	24(14)	176	3.9	0.17	7.2
J1251−7407	0.327	14	3	32.6	0.24(1)	23(1)	6(2)	6(1)	−121(9)	89	2.4	−1.66	7.2
J1331−5245	0.648	43	27	31.9	0.32(2)	30(1)	16(1)	17(1)	83(5)	148	4.2	0.69	7.3
J1409−6953	0.529	31	24	32.4	0.26(2)	16(1)	−4(2)	8(1)	−30(10)	171	4.6	−0.22	7.0
J1432−5032	2.035	52	33	31.4	0.29(2)	18(1)	4(1)	4(1)	11(3)	113	2.8	0.13	6.7
J1443−5122	0.732	117	47	31.5	0.68(3)	22(1)	1(1)	2.6(9)	43(6)	87	1.9	0.61	7.5
J1517−4636	0.887	27	16	32.1	0.37(1)	19.6(9)	5(1)	5.0(8)	−68(7)	126	3.1	−0.66	6.8
J1530−6336	0.91	11	32	31.6	0.43(1)	22.3(8)	16(1)	16.7(7)	202(11)	201	4.9	1.24	7.2
J1534−4428	1.221	178	14	30.6	0.55(3)	28(1)	−2(1)	3(1)	24(6)	137	3.9	0.22	8.0
J1551−4424	0.674	129	27	31.4	1.14(3)	17.1(6)	2(1)	3.2(6)	−32(5)	66	2.4	−0.6	7.8
J1552−6213	0.199	7	3	32.1	0.34(2)	24(1)	0(1)	1(1)	42(14)	122	2.66	0.43	8.1
J1612−5805	0.616	22	4	32.2	0.31(2)	16(1)	3(1)	9(1)	−21(12)	172	3.6	−0.15	7.0
J1614−3846	0.464	45	17	32.6	0.18(2)	31(2)	3(3)	3(2)	45(9)	111	2.7	0.51	6.9
J1622−3751	0.731	48	24	32.4	0.20(1)	30(1)	7(2)	9(1)	85(7)	154	3.9	0.69	6.7
J1626−6621	0.451	39	3	32.5	0.19(2)	20(1)	12(3)	14(1)	39(12)	84	2.2	0.58	7.0
J1627−5936	0.354	159	85	30.8	1.62(4)	22.2(6)	1.3(9)	7.0(6)	89(5)	99	2.2	1.11	8.9
J1629−3636	2.988	41	12	31.0	0.20(2)	29(1)	2(2)	2(1)	0(4)	101	2.4	−0.001	6.8
J1648−6044	0.584	31	12	31.9	0.66(2)	19.7(7)	0(1)	0.3(6)	59(3)	106	2.6	0.69	7.3
J1705−5230	0.231	14	21	32.2	0.60(2)	15.3(9)	1(1)	4.8(8)	−38(9)	170	3.95	−0.28	7.9
J1705−6135	0.809	85	43	30.6	0.30(3)	36(2)	2(3)	4(1)	86(7)	106	2.9	1.0	8.4
J1709−4401	0.865	12	24	32.7	1.15(3)	21.5(5)	7.9(8)	7.9(5)	−122(2)	225	4.4	−0.67	6.3
J1710−2616	0.954	393	99	30.0	1.40(5)	32.5(8)	2(1)	4.4(7)	−9(3)	111	2.6	−0.1	8.9
J1744−5337	0.356	49	18	32.2	0.39(2)	20(1)	3(1)	4.1(8)	52(6)	124	3.6	0.52	7.5
J1749−4931	0.446	8	13	32.4	0.15(1)	9(1)	3(2)	3(1)	42(21)	52	1.4	1.00	7.1
J1802−3346	2.461	77	120	30.5	0.20(2)	28(2)	1(3)	1(2)	236(17)	217	5.4	1.35	7.5
J1805−2948	0.428	22	10	32.4	0.18(1)	16(1)	1(2)	1(1)	23(21)	167	3.77	0.17	7.2
J1811−4930	1.433	39	11	31.5	0.46(2)	23.2(8)	−8(1)	11.0(8)	42(6)	44	1.2	1.19	7.0
J1846−4249	2.273	67	60	30.6	0.29(1)	13.6(9)	8(1)	8.0(8)	82(10)	62	1.8	1.63	7.5

Table 2. Pulsars for which no RM can be determined. Parameters and errors like in Table 1.

Name	P (s)	W_{10} (ms)	W_{50} (ms)	Log $\dot{E}$	S0 (mJy)	L per cent	V per cent	$\|V\|$ per cent	DM (pc cm^{-3})	Log τ_C
J0919−6040	1.217	52	26	29.3	0.23(1)	2(1)	7(1)	7(1)	82	9.3
J1054−5946	0.228	29	7	32.8	0.23(2)	5(2)	3(2)	5(1)	253	7.2
J1143−5536	0.685	24	12	31.8	0.25(1)	0(1)	2(1)	2(1)	185	7.3
J1346−4918	0.3	18	10	31.7	0.70(2)	6.9(6)	3.9(9)	5.6(5)	74	8.1
J1416−5033	0.795	25	12	31.0	0.13(1)	14(2)	0(3)	3(2)	58	8.0
J1539−4835	1.273	91	18	31.4	0.21(2)	0(1)	2(3)	8(1)	118	7.2
J1607−6449	0.298	19	3	31.6	0.22(2)	10(1)	−6(2)	12(1)	89	8.3
J1625−4913	0.356	23	9	33.8	0.22(2)	1(2)	2(3)	2(2)	720	5.9
J1634−5640	0.224	15	8	32.2	0.24(2)	2(1)	1(2)	3(1)	149	7.9
J1647−3607	0.212	15	5	32.7	0.17(2)	11(2)	−2(4)	2(2)	222	7.4
J1700−4422	0.756	72	45	30.6	0.24(3)	6(2)	9(4)	11(2)	413	8.5
J1705−4331	0.223	23	6	32.4	0.43(2)	3(1)	3(1)	3(1)	185	7.7
J1716−4711	0.556	15	4	32.3	0.31(2)	5(1)	6(1)	19.3(9)	287	7.0
J1733−5515	1.011	69	45	31.3	0.38(3)	6(1)	0(2)	1(1)	84	7.5
J1745−3812	0.698	24	11	32.4	0.28(2)	11(1)	5(2)	5(1)	160	6.7

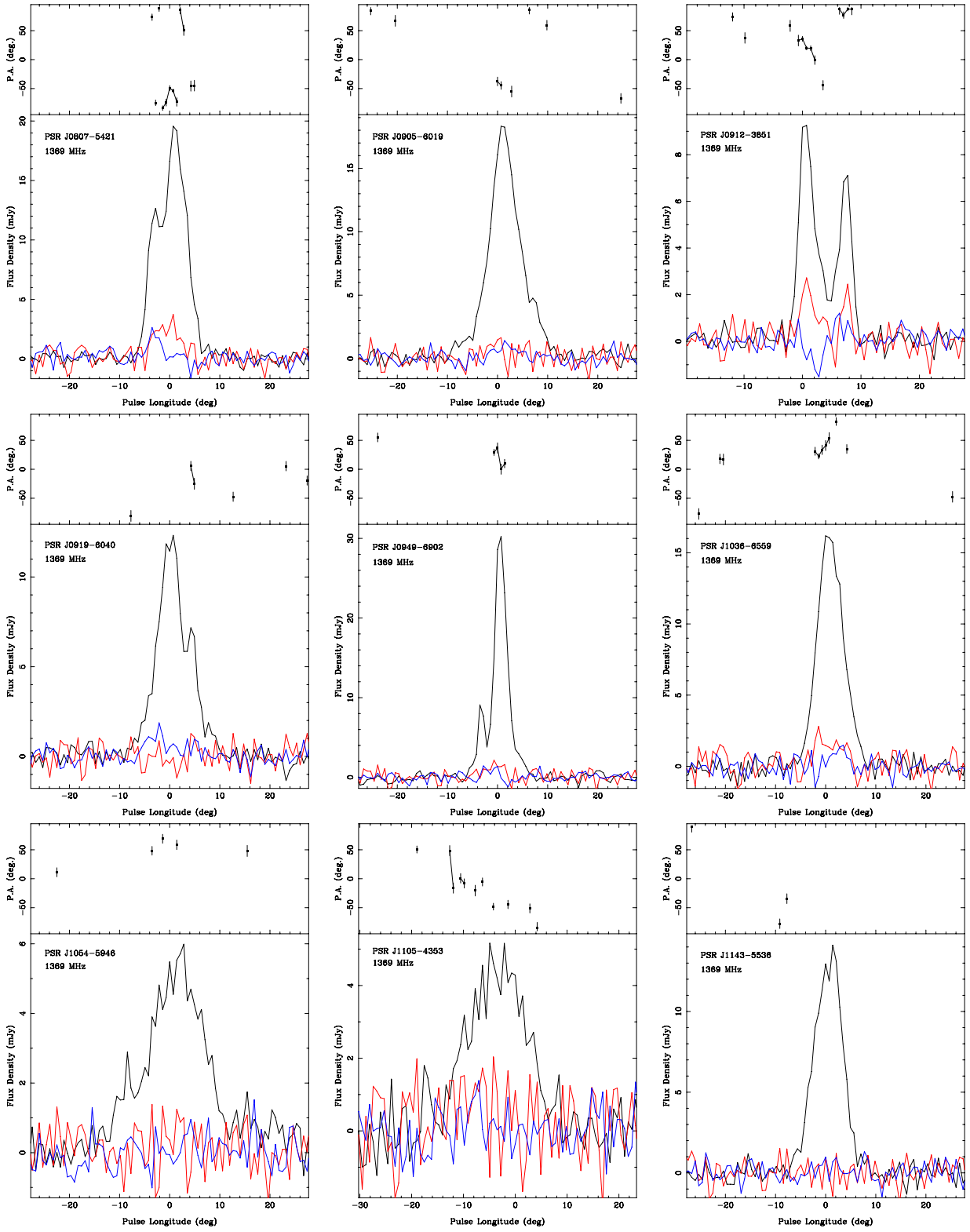

Figure 1. Polarization profiles at 1369 MHz for the pulsars in the sample. The top panel of each plot shows the PA variation with respect to celestial north as a function of longitude. The PAs are corrected for RM and represent the (frequency-independent) value at the pulsar, and are plotted if the linear polarization is above 2σ. The lower panel shows the integrated profile in total intensity (thick black line), linear polarization (red line) and circular polarization (blue line).

3 POLARIMETRIC RESULTS

The main results are given in Tables 1 and 2 along with the full Stokes profiles of the pulsars in Fig. 1. Table 1 includes information for pulsars for which we are able to determine the RM and Table 2 contains the sample for which RMs were not constrained. We can notice from Tables 1 and 2 that only ∼9 per cent of the pulsars with a computable RM show a DM value higher than 200 pc cm^{-3}. On

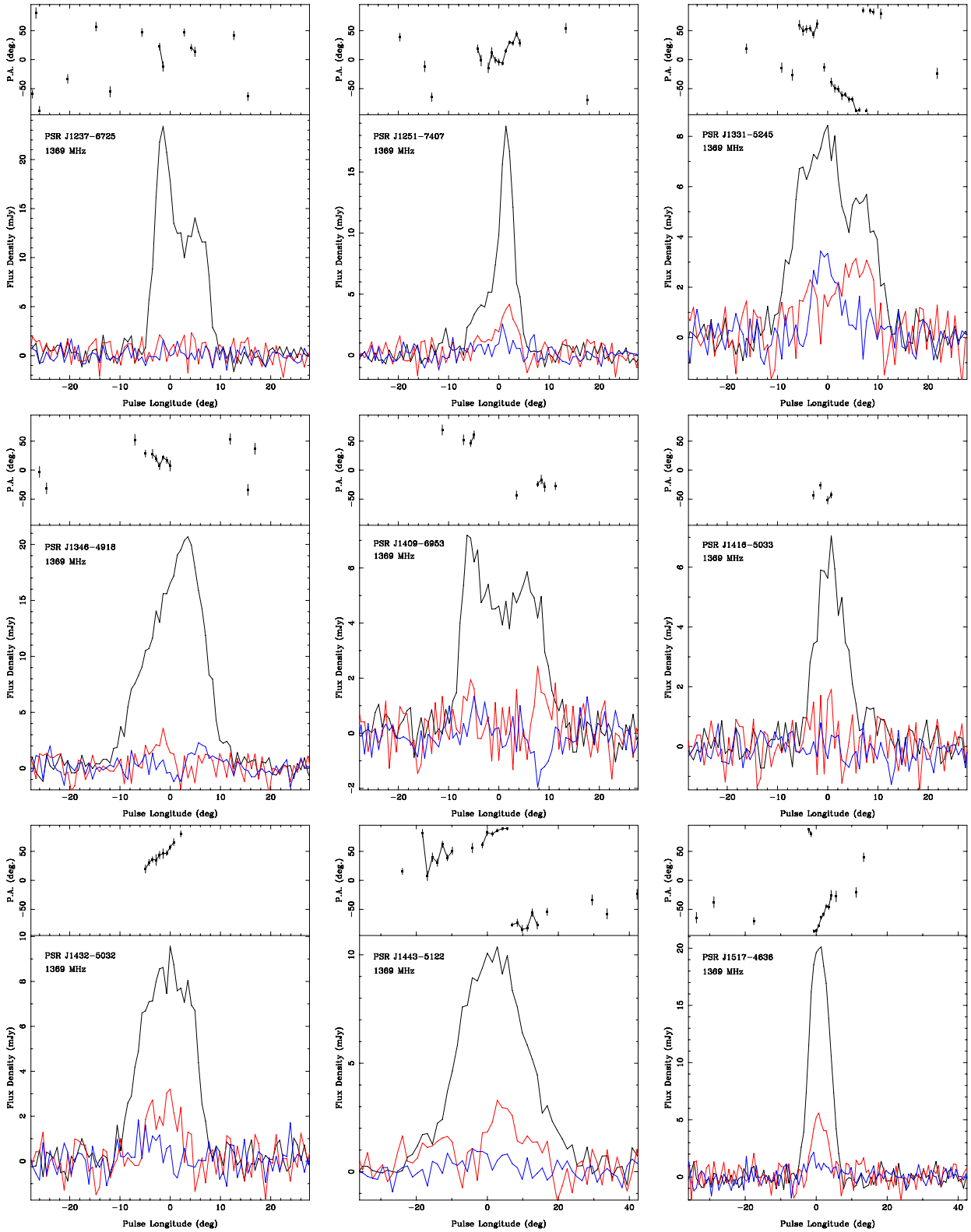

Figure 1 – *continued*

the other hand, ∼33 per cent of the pulsars for which we have not been able to compute a RM exhibit DM > 200 pc cm^{-3}. This is not totally unexpected: in fact, large values of DM can be associated with high values of RM, provided a uniform field is present along the line of sight. Collapsing the total bandwidth in four sub-bands, as we did to obtain the RM, will depolarize the signal if the RM is large enough (note that the low SNR of the pulsars in our sample forces us to not increase the number of sub-bands). For the high-DM pulsars, we attempted a different method for computing RM which involved a search in RM space to maximize for linearly

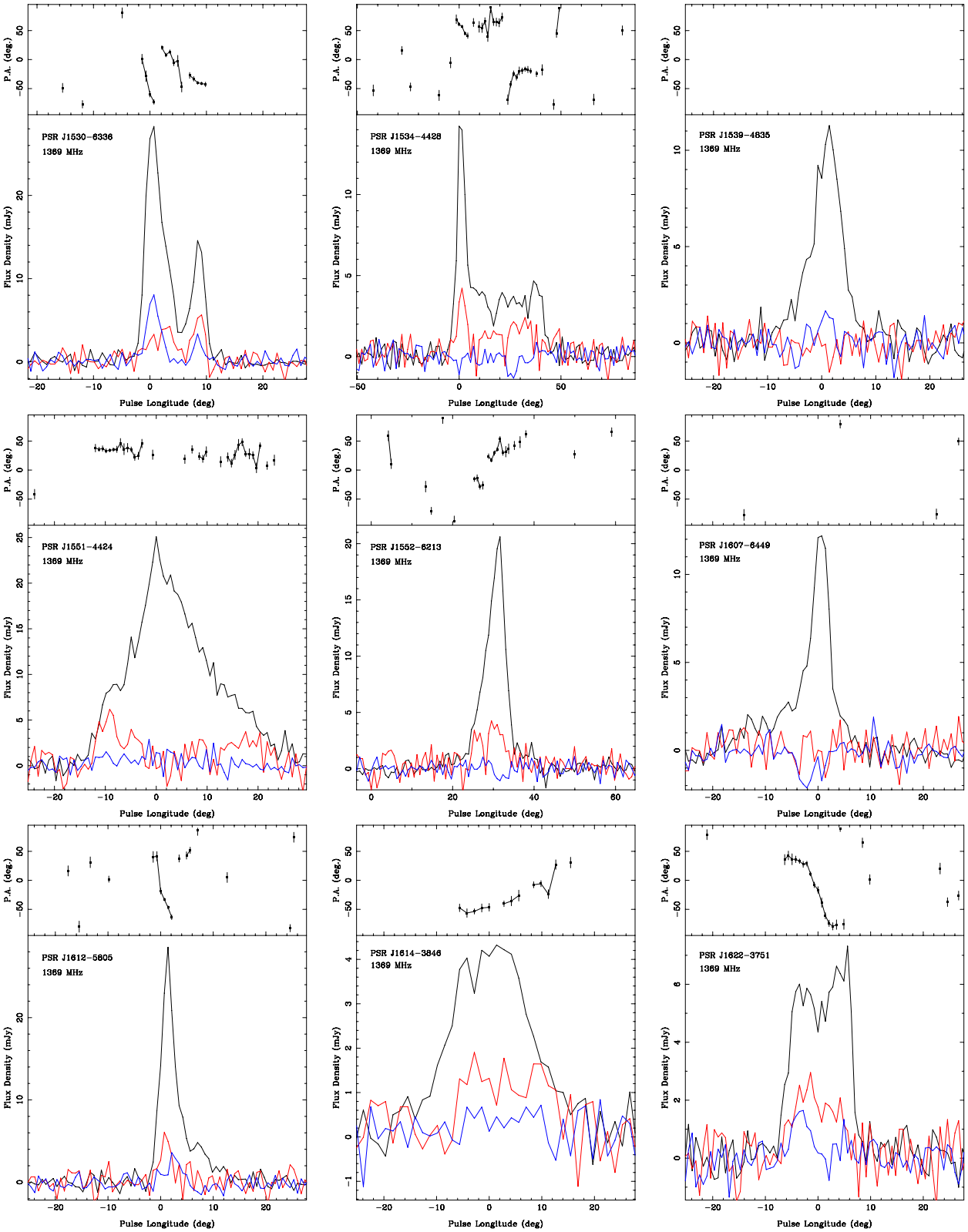

Figure 1 – *continued*

polarized flux. Unfortunately, the low SNR of the pulsars meant that we were unable to determine a reliable RM in any of the cases.

Below, we briefly give a qualitative description of the profiles in total power, linear and circular polarization and the PA curves of the analysed pulsars, except for PSRs J0919−6040, J1054−5946, J1143−5536, J1539−4835, J1625−4913, J1634−5640, J1647−3607 and J1700−4422, for which we were not able to obtain a RM value, and that show very low linear and circular polarization and no interesting features.

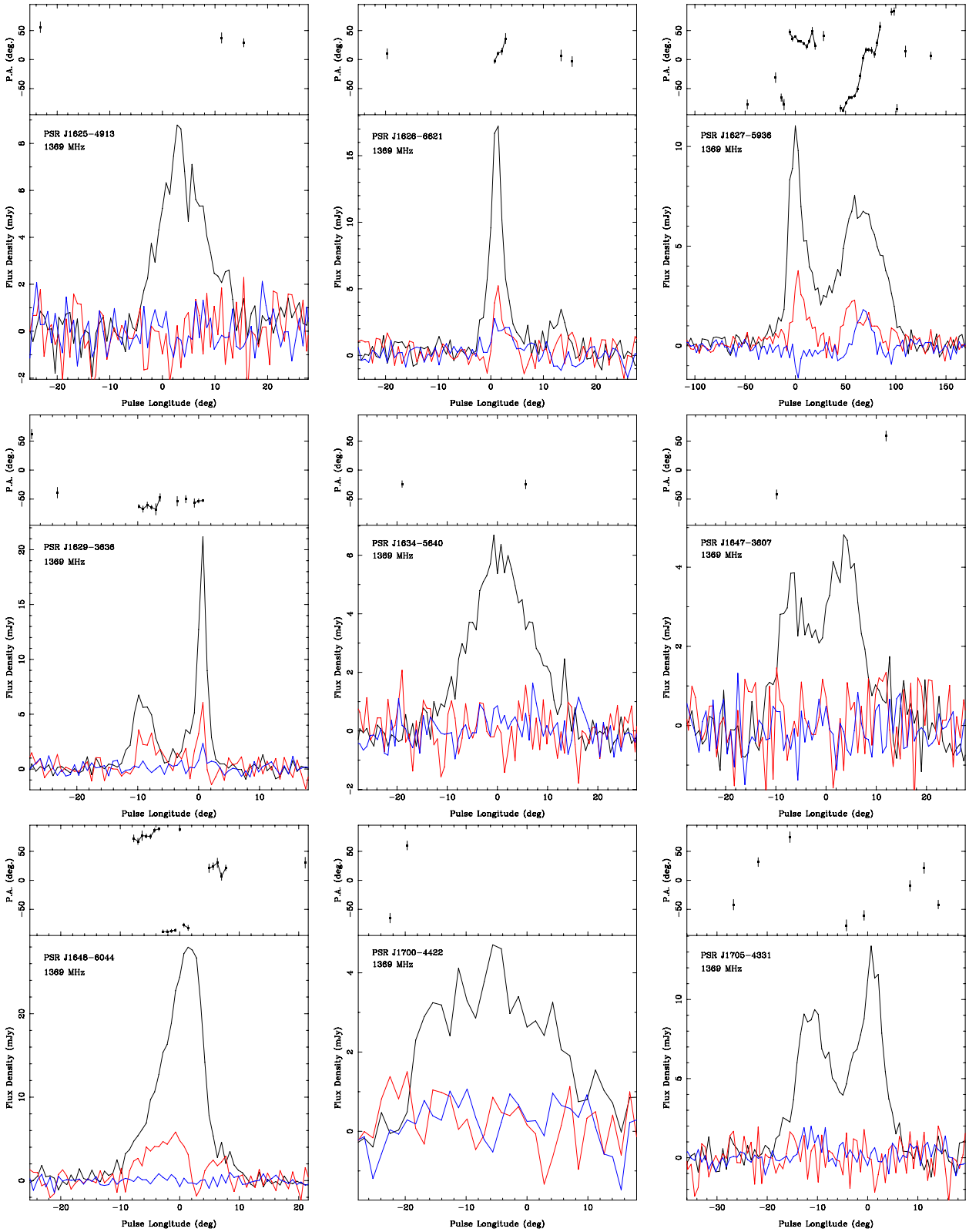

Figure 1 – *continued*

J0807−5421. The profile is relatively narrow, but the total intensity shows two clear, though blended components, with the trailing being the brightest. In contrast, the linear polarization peaks in the centre of the profile and is significantly narrower than the total intensity. The circular polarization displays a sign change towards the trailing component. The PA curve does not exhibit the swing expected from the RVM, but rather a sort of an arch.

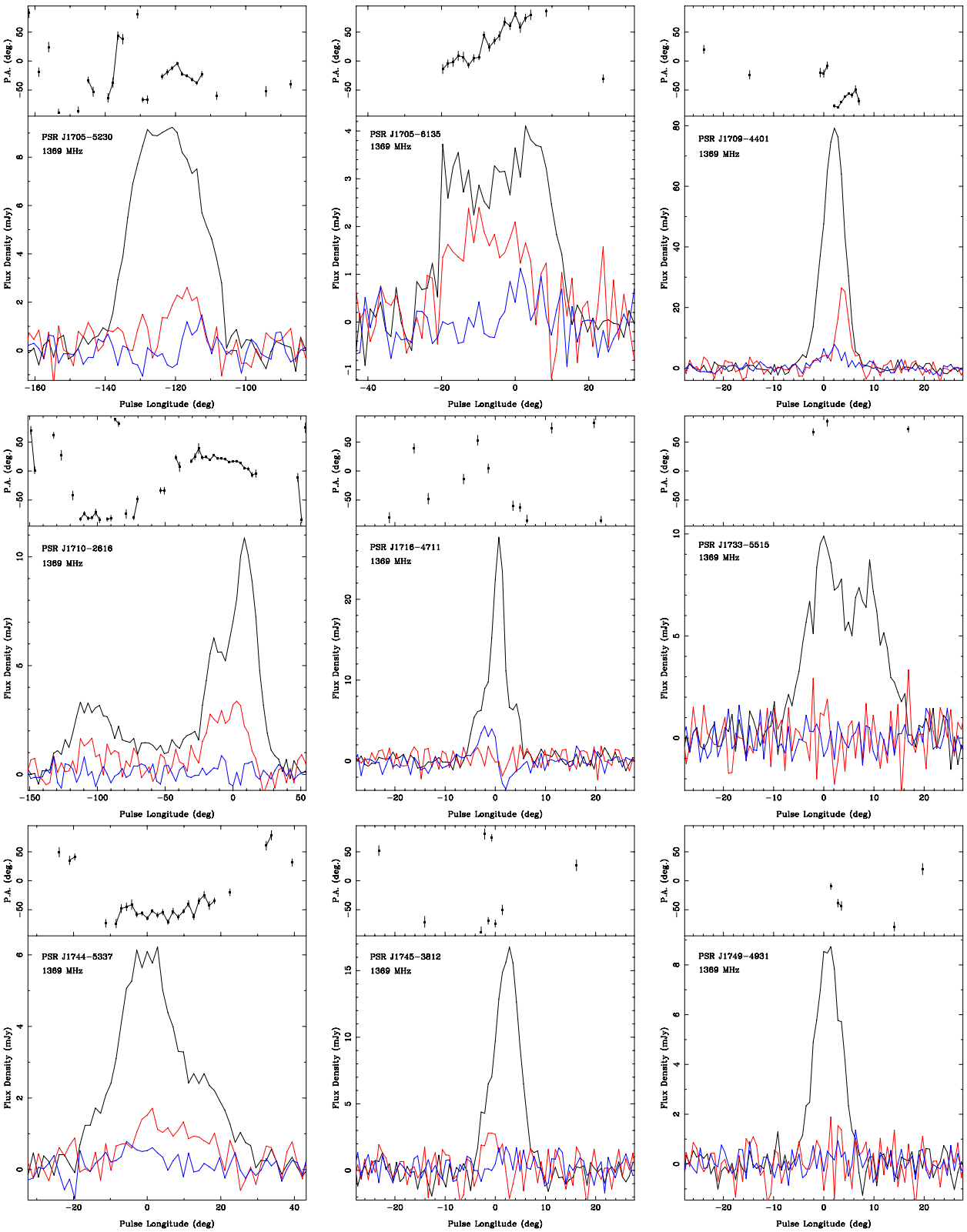

Figure 1 – *continued*

J0905−6019. The profile is relatively narrow and it shows an asymmetric single peak. Although the linear polarization is low, we were able to derive a RM. The circular polarization is faint and left-handed.

J0912−3851. The profile shows two distinct, narrow components, with the leading component being brighter than the trailing one. The linear polarization also shows two peaks, narrower than in total intensity. The circularly polarized signal displays a sign change in

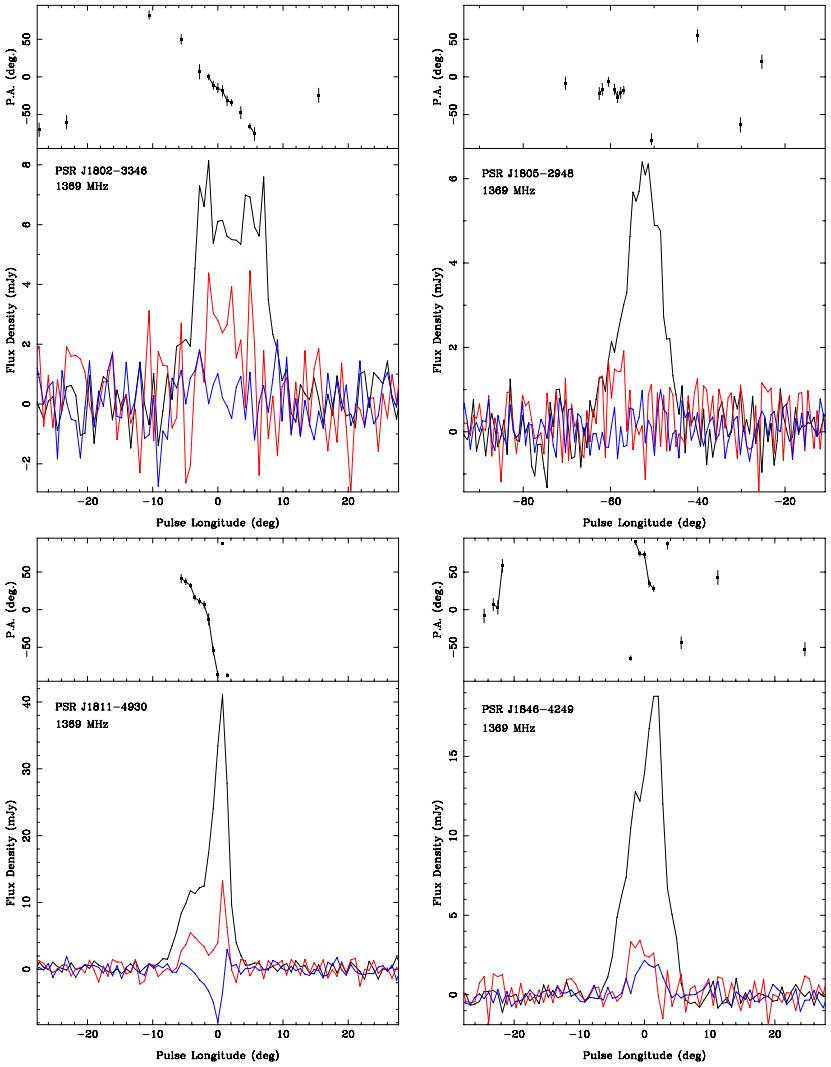

Figure 1 – *continued*

the centre of the profile. We computed a RM value for each of the linear polarization peaks and we found them to be compatible with only overlapping the extremes of the respective 1σ error bar.

J0949−6902. This bright integrated profile shows two almost completely blended, relatively narrow components. The linear polarization is faint, and the circular polarization exhibits a change of sign in the profile centre.

J1036−6559. The total intensity, the linear and the circular profiles all show a single component. The PA curve appears to increase with the phase longitude, and to decrease at its very end.

J1105−4353. The total intensity is noisy and single-peaked. The linear polarization is noisy as well, and the circular polarization is basically absent. The PA curve has no real pattern.

J1237−6725. The profile shows two blended components, with the leading component being the brightest. There is a faint signature of the presence of linear polarization. Note that the observations were folded with a period that is half the real one, which was discovered at a later time. This can have affected the quality of the observations.

J1251−7407. The total intensity profile is narrow and asymmetric, made of at least three blended components. Linear and circular polarization appear to be significant under the trailing component. The PA profile presents three changes of slope in the first half of the pulse profile. After that, it follows a smooth swing with a positive slope that covers about 50° before changing the sense of the slope at its very end.

J1331−5245. This noisy profile shows at least two blended components, where the leading is the brightest. The linear and circular polarization profiles follow the total intensity to a large extent. However, the linear polarization is larger under the leading component whereas the circular polarization is more significant under the trailing components. The PA profile is flat along the leading component, and it shows a steep swing with a negative slope across the trailing one covering about 100°. An almost orthogonal jump occurs between these two parts of the PA profile.

J1346−4918. The profile shows a single, asymmetric component. The circular polarization exhibits a sign change against the maximum of the total intensity profile. The PA profile presents a very smooth decrease in the first half of the pulse profile.

J1409−6953. This noisy total intensity profile is box-shaped. It is perhaps a blended double, although this could be an effect of the occurrence of more than two components. The linear polarization is as well noisy and the PA values have no real pattern. The circularly polarized profile exhibits a right-handed maximum against the profile trailing component.

J1416−5033. This noisy profile shows at least two components, whereof the leading one is the brightest. The linear polarization profile is noisy, and there is no hint of circularly polarized signal.

J1432−5032. The total intensity profile is box-shaped. The linear polarization is noisy but significant, and the left-handed circularly polarized profile is mainly present close to the leading edge of the total intensity curve. The PAs exhibit a smooth swing across the profile covering about 70°. Note that the observations were folded with a period that is half of the real one, discovered at a later time. This can have affected the quality of the observations.

J1443−5122. This noisy and relatively broad profile is asymmetric and shows a single component. The linearly polarized profile is significant when close to the leading edge, and another peak occurs at the centre of the profile. There is almost no circular polarization. The PAs exhibit a smooth swing with a positive slope, covering about 120°.

J1517−4636. The profile displays a narrow, single component. The linear polarization largely follows the total intensity but it is narrower. The PA curve exhibits a change of slope close to the leading edge of the pulse profile, followed by a steep swing with a positive slope, that extends over ∼50°.

J1530−6336. The total power profile shows two principal components, with the leading being the brightest. The circular polarization follows the total power, but it is narrower. On the contrary, the linear polarization is characterized by at least three components. The first two of them are almost blended and occur before the trailing peak of the total intensity profile. The PAs show two swings with similar slopes under the two leading components of the linear polarization. They are separated by an OPM jump. The third part of the PA profile is a swing with a flatter slope.

J1534−4428. The total intensity profile extends over more than 40° and consists of a bright leading component followed by a flat structure. There is a significant degree of linear polarization which largely tracks the total intensity profile. If we interpret this structure as a zone of partially overlapping components, the depolarization can be explained thanks to the fact that the linearly polarized profile is narrower than the total power one. The PA curve is largely flat but rises steeply in the middle of the profile before flattening off again.

J1551−4424. This profile is affected by interstellar scattering, and it shows a typical steep rising edge to a peak followed by a more gradual decay. The small linear polarization fraction is concentrated towards the leading edge of the profile. The PA swing is remarkably flat, an effect that is induced by the scattering (Li & Han 2003).

J1552−6213. The total intensity profile is single-peaked and slightly asymmetric, with the trailing edge being steeper than the leading. The circular polarization is barely visible and slightly right-handed in the second part of the profile. The linear polarization shows two components, with the brightest roughly corresponding to the maximum of the total power. The first part of the PA profile is followed by a non-orthogonal jump. The second part shows a generally rising trend.

J1607−6449. The profile is made of at least two almost completely blended components. The linear polarization is noisy. There is a significant occurrence of the right-handed, circularly polarized signal, that is mostly present in the first half of the pulse profile.

J1612−5805. The total intensity profile shows three features: a narrow, slightly asymmetric leading component and blended, fainter central and trailing components. The linearly polarized profile is mainly present beneath the leading component, and its peak almost coincides with the maximum of the total power. The circular polarization shows a change of sign between the leading and the central component. The PA curve starts flat and exhibits a very steep swing with negative slope across almost the entire leading peak, followed by a slightly increasing curve towards the centre of the pulse profile. The two parts of the PA profile are separated by a jump of ∼110°.

J1614−3846. The total intensity profile is noisy, box-shaped and symmetrical, and these attributes are largely mirrored by the linear polarization. The circular polarization is almost absent. The PA curve exhibits a smooth swing, with a positive slope that covers about 50°.

J1622−3751. The profile is a blended double with the trailing component being the brightest. The linear polarization, in contrast, is more significant in the leading component. The circular polarization changes sign in the centre of the profile. Unusually amongst this sample, the PA profile shows the classic RVM signature: a flat beginning followed by a wide swing beneath the linearly polarized leading and trailing peaks, and flatter again at the end of the profile. The swing centre coincides with the minimum in the total intensity. It covers about 120°.

Despite the fact that the pulse profile is narrow, the steep swing of PA lends itself to the RVM fitting. We find that, although the angle between the spin and magnetic axis is unconstrained, the impact angle must be less than 4°. Interestingly also, the inflexion point of the RVM (the magnetic pole) aligns with the midpoint of the profile to within 0°.5. The lack of significant offset implies a low emission height of less than 100 km. Such a low emission height favours a non-orthogonal rotator with preferred values of $\alpha \lesssim 40°$.

J1626−6621. The profile shows two distinct, relatively narrow components, with the leading component being significantly brighter. The linear and the circular polarizations occur in correspondence of the profile's leading component. The PA profile exhibits a steep swing across this peak, which covers about 50°.

J1627−5936. This broad profile extends over more than 100° of longitude. It shows an asymmetric, relatively narrow leading component followed by a central structure and a broader and fainter trailing component that is probably a blended double. The linear and circular polarization profiles roughly follow the total power. However, while all three approximately peak at the same longitude in the leading component, in the trailing one the maxima of linear and circular polarisations are shifted. In the central structure, both circular and linear depolarizations occur. A change of handedness is displayed by the circular polarization between the two main components. The PAs are mainly flat beneath the leading component, and show a swinging behaviour compatible with the RVM predictions in correspondence of the trailing component.

J1629−3636. The total power shows two peaks, with the asymmetric trailing being the brightest and narrowest. The linearly polarized profile mirrors the total intensity but it is narrower, while the

circular polarization is visible just in correspondence of the trailing component and it is left-handed. The PA profile is flat for both of the linearly polarized components.

J1648−6044. The profile has a single, asymmetric peak. However, the linear polarization displays two clear components. The PA curve starts with a smooth swing that covers about 50°, and continues with an almost orthogonal jump between the two components of the linearly polarized profile. The last part of the PAs value is practically flat.

J1705−4331. The profile shows a classic double structure with the trailing component slightly brighter than the leading component. There is some circular polarization in the leading component.

J1705−5230. The profile is relatively broad and box-shaped, possibly a blend of several components. The linear polarization shows a first, weak peak followed by a brighter one close to the total power trailing edge. In correspondence of the main, linearly polarized component, the PAs exhibit a practically flat trend.

J1705−6135. The profile is noisy, broad and box-shaped, and it is possibly a blended double. The fraction of linear polarization is relatively high, particularly against the leading part of the profile. The PA curve exhibits a smooth swing across the profile, with a positive slope that covers ∼130°.

J1709−4401. The profile of this intermittent pulsar shows a single, relatively narrow and pretty symmetrical peak. The linear polarization has a main component close to the total intensity trailing edge, and it shows a hint of a minor peak on the leading side. The flux density is about one third of the total power one, and their maxima are misaligned. The circular polarization is scarce and noisy. Beneath the weak leading component in the linearly polarized profile, the PA curve starts flat and follows a steep trend with a positive slope. The PA profile under the main linear polarization peak is separated from the leading one by an almost orthogonal jump. It has a flat start too, followed by two swings with positive and negative slopes, respectively.

J1710−2616. This broad profile shows emission over nearly 180° of longitude. A broad leading component is followed by a bridge of emission linking it to a blended double. The linear polarization mostly follows the total intensity but the circular polarization remains low throughout. Although the low linear polarization in the profile centre, the characteristic S-shape from the RVM is recognizable. In fact, the large longitude coverage of the pulse profile and the smooth PA swing lends itself well to RVM fitting. Results show that α must be less than 30°, with an impact parameter of ∼20° or less. The location of the inflexion point of the RVM is coincident with the profile centre. The pulsar therefore appears to be an almost aligned rotator.

J1716−4711. The profile shows a single, relatively narrow component possibly flanked by two outriders. The circular polarization displays a clear change of sign in correspondence of the profile centre.

J1733−5515. The profile shows two blended components of almost equal amplitude. Very small linear or circular polarization can be discerned.

J1744−5337. The profile is affected by the interstellar scattering. It shows a broad and asymmetric leading component blended with a second one. The linear polarization profile is significant especially in the second half of the pulse profile. The PA curve is flat.

J1745−3812. The profile shows a single and slightly asymmetric component with low circular polarization. In spite of a moderate degree of linear polarization, we were not able to obtain a RM value for this pulsar.

J1749−4931. This single-peaked profile shows no clear signs of circular polarization, while the linear polarization is present but weak.

J1802−3346. This noisy and box-shaped profile shows at least two blended components. The linear polarization profile follows the total intensity but it is narrower, and the PA curve displays a swing with negative slope that covers ∼90°.

J1805−2948. This noisy profile shows a single, relatively broad and asymmetric component. There appears to be a linearly polarized component on the leading edge of the profile with a flat PA swing.

J1811−4930. The profile of this intermittent pulsar is a blended double with the trailing component brighter. The linear polarization follows the total power, though it is narrower. On the other hand, the circular polarization peaks where L is fainter. The PA profile shows a steep swing with negative slope in correspondence of the leading component that covers about 130°, while it is flat beneath the trailing.

J1846−4249. This profile shows two blended peaks. The linear and circular polarizations, however, exhibit a single, box-shaped component at the centre of the pulse profile. The PA curve shows a steep swing spanning 80°.

4 DISCUSSION

In our sample, the percentage of the linear polarization, L per cent, ranges from a few per cent to almost 40 per cent. However, only two of the sources (PSR J1614−3846 and PSR J1705−6135) approach the aforementioned upper limit: the mean of L per cent is ∼16.

The dependence of L per cent on the pulsar spin-down luminosity is:

$$\dot{E} \simeq 3.95 \times 10^{31} \mathrm{ergs}^{-1} \left(\frac{\dot{P}}{10^{-15}}\right) \left(\frac{P}{s}\right)^{-1} \tag{11}$$

where $\dot{P}$ is the spin period derivative (Lorimer & Kramer 2005), is reported by von Hoensbroech & Xilouris (1997), Crawford, Manchester & Kaspi (2001) and Johnston & Weisberg (2006). These authors noticed that higher values of $\dot{E}$ gave higher values of L per cent. This trend was better modelled by Weltevrede & Johnston (2008), who found that the correlation between the two quantities is not linear. They identified two main regions, a low $\dot{E}$ (less than 5×10^{33} erg s^{-1}), low L per cent (less than 50 per cent) area and a high $\dot{E}$ (more than 2×10^{35} erg s^{-1}), high L per cent (exceeding 50 per cent) one, divided by a narrow transition zone. As can be seen from Fig. 2, the results derived from our low $\dot{E}$ sample do not conflict with Weltevrede & Johnston (2008): all of the pulsars (except one) belong to the low $\dot{E}$ interval and show L per cent smaller than 40 per cent. Moreover, no clear correlation of L per cent versus $\dot{E}$ is present over the low $\dot{E}$ sample.

In Fig. 3 we show the characteristic age, τ_{C}:

$$\tau_{\mathrm{C}} = \frac{P}{2\dot{P}} s \tag{12}$$

plotted versus L per cent and $|V|$ per cent (that is the percentage of the absolute circular polarization) and compare our results with

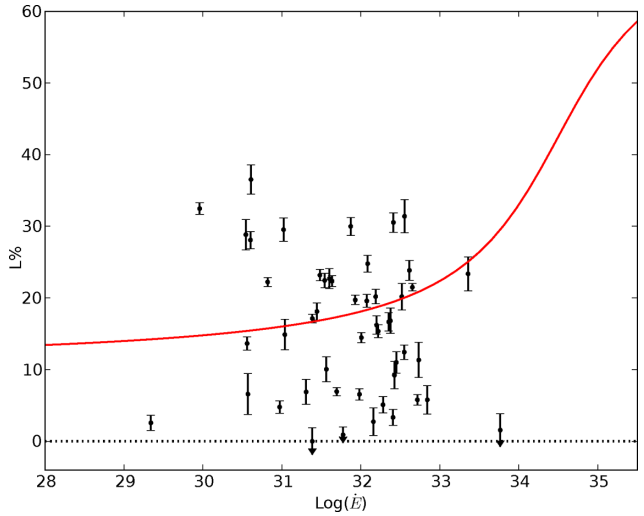

Figure 2. Percentage of linear polarization against the spin-down luminosity $\dot{E}$. The black points represent the individual pulsars of our sample with 1 σ error bars (the arrows imply an upper limit), while the red line is the fit reported in Weltevrede & Johnston (2008).

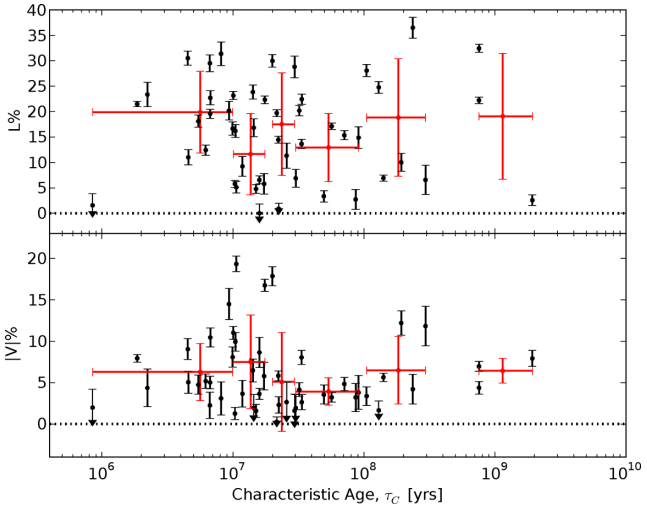

Figure 3. Percentage of linear polarization against the characteristic age in the top panel, and percentage of absolute circular polarization against the characteristic age in the bottom panel. The black points represent the individual pulsar of our sample with 1σ error bars (the arrows imply an upper limit), while the red points and the vertical and horizontal bars represent the average over suitable groups of pulsars, the scatter and the range of age involved in the computation of the mean, respectively.

Gould & Lyne (1998). Since τ_C of the pulsars in our sample (except PSR J1625−4913) exceeds 1 Myr, according to the results of Gould & Lyne (1998), values of L per cent around 20 per cent are expected. Although a large degree of scatter is present in the sample, the average values of L per cent are in fact between 10 and 20 per cent. Regarding the percentage of $|V|$, we find a less pronounced degree of scatter in the data, and generally lower values of the average $|V|$ per cent with respect to the results of Gould & Lyne (1998). We expected values around 8 per cent for 10^6 Myr $\leq \tau_C \leq 10^7$ Myr, and slightly higher results for older ages. We instead find a generally flat trend when the values of $|V|$ per cent are averaged over the six bins in τ_C, into which our sample has been split. In particular, the average $|V|$ per cent is $\sim 6 \pm 3$ for pulsars with $\tau_C \geq 10^7$ Myr yr, fully compatible with the value of $\sim 6 \pm 5$ for pulsars with $\tau_C \leq 10^7$ Myr yr.

For the majority of the pulsars in our sample, we can recognize the presence of more than one component in the profiles. This is not unexpected since pulsars of an advanced age typically have more complicated profiles than younger objects (Rankin 1983; Lyne & Manchester 1988; Rankin 1993; Johnston & Weisberg 2006; Karastergiou & Johnston 2007). Karastergiou & Johnston (2007) attribute this evidence to the location of the emitting regions crossed by the line of sight, assuming that each of them corresponds to one component in the profile. In particular, at a fixed observing frequency, the radio emission in young pulsars should be produced from a limited range of altitudes above the neutron star surface. This range widens and descends to lower heights in the magnetosphere with increasing age of the pulsar. According to the model presented by Karastergiou & Johnston (2007), this naturally increases the number of emitting regions crossed by the observer line of sight, and hence the number of components in the profile. A large fraction of the profiles in our sample show a blended double, i.e. the superposition of two main components that ranges from barely distinguishable (as in PSR J0807−5421) to well (as in PSR J0912−3851) visible. There is also a tendency for the trailing component to be brighter than the leading one. According to the literature (i.e. Rankin 1983), a double component profile should indicate a mainly conal emission. Emission structures that are not well-defined are also observed, the clearest example of which is for PSR J1534−4428. Emission bridges are also exhibited among otherwise separated components, as in PSRs J1627−5936 and J1710−2616. Given the relatively small SNR of the majority of the pulsars, it is not easy to distinguish the occurrence of multiple components from the case of pure double profiles. Nevertheless, some objects certainly show at least three components, e.g. PSRs J1251−7407, J1607−6449 and J1802−3346.

The linear polarization, when present, follows the total intensity in the majority of the cases, although it often shows a general edge depolarization that causes a narrowing in the polarization profile, as illustrated in PSRs J1517−4636 and J1811−4930. The phenomenon of the linear depolarization is usually explained via the superposition of two emission modes that are in competition in pulsars (Stinebring et al. 1984).

The circular polarization profiles are often barely visible, but show some cases of change in handedness between the components (as in PSRs J0807−5421, J1612−5805, J1627−5936) or across the profile (as in PSRs J1346−4918 and J1716−4711).

As mentioned in Section 2, in those pulsars (nine over the total sample of 34 objects for which RM has been determined) that show more than one peak in the linear polarization profile, we separately fit for the RM component by component. In the majority of the cases, we obtained fully compatible (at 1σ) RM values. In PSRs J0912−3851 and J1629−3636 the agreement is marginally accomplished only by the overlap of the extremes of the respective 1σ uncertainties intervals. However, this is expected on a statistical bases given the available sample of nine sources.

4.1 Pulsars RM and Galactic magnetic field

We have collected all the sources discovered so far by the HTRU southern survey and having a measured value of RM. The list totals 51 pulsars, resulting from the present work, as well as from Bailes et al. (2011); Keith et al. (2012) and Burgay et al. (2013). These values can be used to obtain an estimate of the average intensity and

sign of the projection of the Galactic magnetic field vector ($\langle B_{||} \rangle$) along the 51 lines of sight to the pulsars. In fact, the RM is defined as:

$$\mathrm{RM} = \frac{e^3}{2\pi {m_\mathrm{e}}^2 c^4} \int_0^d n_\mathrm{e}(l) B_{||}(l) \mathrm{d}l \tag{13}$$

where e is the electron charge, m_e is the electron mass, d is the distance between the emitting object and the observer, n_e is the electron column density and $B_{||}$ is the projection of the magnetic field vector along the line of sight. Since the DM is defined as

$$\mathrm{DM} = \int_0^d n_\mathrm{e}(l) \mathrm{d}l \tag{14}$$

is it possible to obtain $\langle B_{||} \rangle$ as

$$\begin{aligned} \langle B_{||} \rangle &= 1.232 \frac{\int_0^d n_\mathrm{e}(l) \mathrm{B}_{||}(l) dl}{\int_0^d n_\mathrm{e}(l) \mathrm{d}l} \\ &= 1.232 \left(\frac{\mathrm{RM}}{\mathrm{m^{-2}rad}} \right) \left(\frac{\mathrm{DM}}{\mathrm{cm^{-3}pc}} \right)^{-1} \mu\mathrm{G}. \end{aligned} \tag{15}$$

The resulting values of $\langle B_{||} \rangle$ are reported in the second last column of Table 1. For each of the considered objects, we also derived a measurement of the distance (see Table 1) using the DM value of each object and the NE2001 electron density model (Cordes & Lazio 2002). Assuming these distances, all the selected pulsars are located within 2 kpc in height from the Galactic plane and thus the lines of sight to all of them are expected to be useful to investigate the behaviour of the Galactic magnetic field in the proximity of the Galactic disc (Noutsos et al. 2008). In Fig. 4 we have reported the positions – projected on to the Galactic plane – of the objects of our sample.

Our sample does not support the hypothesis suggested by Vallée (2005) of a prevailing counter-clockwise direction of the Galactic magnetic field in an annulus included between 4 and 6 kpc from the Galactic Centre and a prevailing clockwise direction outside the annulus. First, looking at Fig. 4 it is evident the occurrence of opposite signs for the values of RMs for many pairs of pulsars which are very close to each other. As already pointed out by other authors (e.g. Noutsos et al. 2008), this is an indication for

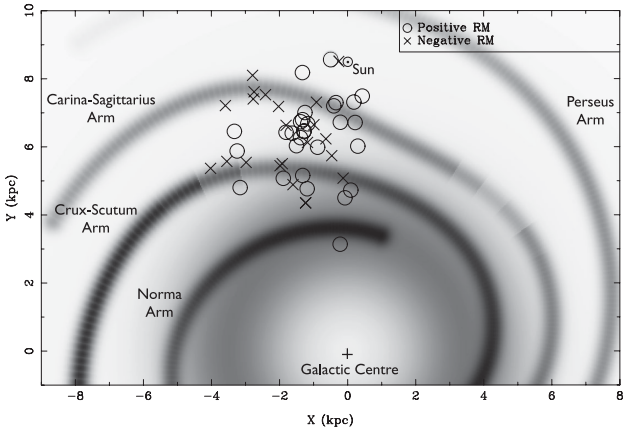

Figure 4. A scheme of the Milky Way seen from the North Galactic Pole. In dark grey are shown the galaxy arms as from Taylor & Cordes (1993). The symbol ⊙ indicates the Sun, the circles and the crosses indicate the pulsars of our sample with positive and negative values of RM, respectively. The distances of the pulsars have been computed using the NE2001 electron model (Cordes & Lazio 2002), prone to errors on the calculated distance up to the 30 per cent

variations of intensity and direction of the Galactic magnetic field also over small scales. To be more quantitative, we also computed (as first suggested by Lyne & Smith 1989) the average intensity of the magnetic field in the intermediate region between pairs of pulsars:

$$\langle B_{||} \rangle_{\mathrm{d_1-d_2}} = 1.232 \frac{\Delta\mathrm{RM}}{\Delta\mathrm{DM}}\ \mu\mathrm{G} \tag{16}$$

where d_1 and d_2 are the distances of the two sources from the Sun and ΔRM and ΔDM are the differences between the RM and the DM values of the two considered pulsars, respectively. In doing that, we followed the prescription of Noutsos et al. (2008), i.e. investigating pairs of pulsars the projected positions of which are closer than 5° in Galactic longitude. For the limited range in distances and Galactic longitudes of our sample, a counter-clockwise direction for the Galactic magnetic field would correspond to a prevalence of positive values of $\langle B_{||} \rangle_{\mathrm{d_1-d_2}}$ for pairs located in the first Galactic quadrant (Galactic longitudes between 0° and 90°) and a prevalence of negative values of $\langle B_{||} \rangle_{\mathrm{d_1-d_2}}$ for pairs in the fourth Galactic quadrant. At variance with the expectations of the model of Vallée (2005), no trend is recognizable in our sample. In particular, within the annulus mentioned above, the values of $< B_{||} >_{\mathrm{d_1-d_2}}$ for six pairs of pulsars are compatible with a counter-clockwise direction of the Galactic magnetic field, whereas a clockwise direction is preferred on the basis of six other pairs. Similarly, the results for 24 pairs of pulsars would favour a clockwise direction for the region outside the annulus, whilst the consideration of 26 other pairs would suggest the opposite direction.[2]

We also performed a preliminary investigation of the compatibility of our sample with the model of Han et al. (2006), which states the occurrence of a counter-clockwise direction for the Galactic magnetic field along the arms and an opposite direction of that in the inter-arm regions. Given the distances of the pulsars in our sample (typically spanning the range 1–4 kpc) and the relatively small number of available objects, our investigation focused on the case of the closest arm, i.e. the Carina-Sagittarius arm (see Fig. 4). We then selected those pulsars whose projected position is compatible with them belonging to the area of the Carina-Sagittarius arm or close (within 0.5 kpc) to that. That choice left us with 13 objects, whose Galactic longitudes span the range between −82° and 23°. Adopting the same criteria as mentioned above, eight pairs of pulsars can be selected in this region and the related values of $\langle B_{||} \rangle_{\mathrm{d_1-d_2}}$ measured. It results in a prevalence of pairs (6 vs 2) indicating a counter-clockwise direction of the Galactic magnetic field along the Carina-Sagittarius arm, nominally in agreement with the model of Han et al. (2006). Fig. 5 indicates that some large-scale ordered component of the Galactic magnetic field can indeed be present in the Carina-Sagittarius arm, being reflected in the overall trend for the RM values, which change from positive to negative values with increasing values of DM. Unfortunately our sample is not suitable to test the detailed dependence of RM versus DM inferred by Han et al. (2006) for the objects belonging to the Carina arm and having DM < 200 pc cm^{-3}, i.e. RM $\propto -$ 0.6DM, for the pulsars with Galactic longitudes between −76° and −68°. In fact Han et al. used only pulsars at Galactic latitude less than |8|°, which are too rare in our sample (resulting from a survey at intermediate and high Galactic latitudes) for a meaningful comparison. However, Fig. 5 also shows that the status of the magnetic field in the Carina-Sagittarius

[2] The total number of pairs is larger than the number of pulsars of our sample since few pulsars of the sample enter more than one pair.

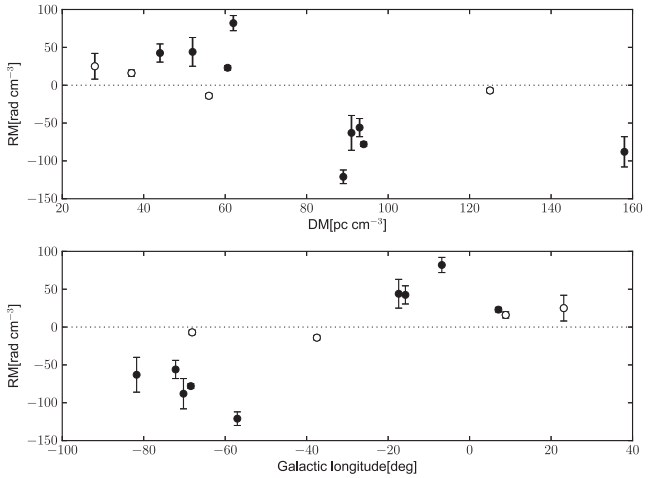

Figure 5. In the top panel are shown the RM values for the pulsars the projected positions of which are in agreement with their belonging to the Carina-Sagittarius arm, plotted in function of their DM. In the bottom panel are shown the RM values for the same pulsars plotted in function of their Galactic longitude. Empty circles indicate pulsars with positive Galactic latitude, whereas filled circles are associated with pulsar located at negative Galactic latitude. 1σ error bars are overlapped to the data points. Note that the error bar associated with some of the data points are too small to be visible.

arm is more complex than described by the relatively simple model of Han et al., with a large scatter of values of RM for similar values of DM and the trend in Fig. 5 which is much more evident for the pulsars below the Galactic plane than for the ones at positive Galactic latitudes. As a consequence, additional components in the Galactic magnetic field are likely needed, like those investigated by Noutsos et al. (2008). A significant improvement in the modelling is expected when the sample presented here will be complemented by the discoveries resulting from the low-latitude part of the HTRU survey (Ng et al., in preparation).

5 SUMMARY

We have presented a polarimetric analysis of 49 long-period pulsars discovered as part of the HTRU southern survey. We were able to compute the RM for 34 of them, while nine objects show almost no polarized signal.

We found that the percentage of L among the pulsars in the sample is mainly around 15–20 per cent, in agreement with previous studies (Gould & Lyne 1998; Weltevrede & Johnston 2008) for sources with $\dot{E}$ lower than 5×10^{33} erg s^{-1} and a characteristic age larger than 1 Myr. In addition, the mean degree of $|V|$ is roughly compatible with expectations, although it does not show any sign of a minimum in the range of ages between 10^6 and 10^7 years as in Gould & Lyne (1998). This can be due to the smaller number of pulsars in our sample. However, we believe that these differences are not significant.

For the majority of the total power profiles, we recognized the presence of more than one component, as expected for a sample of 'old' pulsars. In particular, we note the frequent occurrence of blended-double shaped profiles. According to the literature (i.e. Rankin 1983), this is an indication of a conal emission. The linear polarization profiles often mirror the total intensity shape, although the former are almost always narrower than the latter, as already noticed in Rankin (1983) while the fainter circular polarization profiles show a handedness reversal in a few cases. The PA swings vary from flat behaviours to mode jumps and some occurrences of RVM-like swings. For two of the analysed pulsars, the fit for the swing yields some geometrical constraints on the radio-beam. Both appear to be almost aligned ($\alpha \ll 45^\circ$) rotators.

We have also carried out a preliminary analysis of the Galactic magnetic field resulting from the available sample of pulsars discovered so far in the HTRU southern survey that have a computable RM value, and we studied the implications of the results we obtained. The data do not support the model presented by Vallée (2005), whereas there is some agreement with the one proposed by Han et al. (2006) and Noutsos et al. (2008). In contrast with Vallée (2005), Han et al. (2006) and Noutsos et al. (2008) claim that the Galactic magnetic field has a counter-clockwise direction in the arms and a clockwise direction in between. However, given the limited number of pulsars in our sample and their proximity to the Sun, it is difficult to put significant constraints on more complicated large-scale models for the Galactic magnetic field for the time being.

ACKNOWLEDGEMENTS

The Parkes radio telescope is part of the Australia Telescope which is funded by the Commonwealth of Australia for operation as a National Facility managed by CSIRO. Part of this research was carried out at the Jet Propulsion Laboratory, California Institute of Technology, under a contract with the National Aeronautics and Space Administration. CT also thanks Delphine Perrodin for her help.

REFERENCES

Backer D. C., Rankin J. M., Campbell D. B., 1976, Nat., 263, 202
Bailes M. et al., 2011, Sci, 333, 1717
Bates S. D. et al., 2011, MNRAS, 416, 2455
Bates S. D. et al., 2012, MNRAS, 427, 1052
Beskin V. S., Philippov A. A., 2012, MNRAS, 425, 814
Blaskiewicz M., Cordes J. M., Wasserman I., 1991, ApJ, 370, 643
Burgay M. et al., 2013, MNRAS, 433, 259
Cordes J. M., Lazio T. J. W., 2002, preprint (astro-ph/020715)
Cordes J. M., Rankin J. M., Backer D. C., 1978, ApJ, 223, 961
Crawford F., Manchester R. N., Kaspi V. M., 2001, AJ, 122, 2001
Eatough R. P., Keane E. F., Lyne A. G., 2009, MNRAS, 395, 410
Everett J. E., Weisberg J. M., 2001, ApJ, 553, 341
Gould D. M., Lyne A. G., 1998, MNRAS, 301, 235
Gupta Y., Gangadhara R. T., 2003, ApJ, 584, 418
Han J. L., Manchester R. N., 2001, MNRAS, 320, L35
Han J. L., Qiao G. J., 1994, A&A, 288, 759
Han J. L., Manchester R. N., Xu R. X., Qiao G. J., 1998, MNRAS, 300, 373
Han J. L., Manchester R. N., Qiao G. J., 1999, MNRAS, 306, 371
Han J. L., Manchester R. N., Lyne A. G., Qiao G. J., 2002, ApJ, 570, L17
Han J. L., Manchester R. N., Lyne A. G., Qiao G. J., van Straten W., 2006, ApJ, 642, 868
Hibschman J. A., Arons J., 2001, ApJ, 546, 382
Hotan A. W., van Straten W., Manchester R. N., 2004, PASA, 21, 302
Johnston S., Weisberg J. M., 2006, MNRAS, 368, 1856
Johnston S., Karastergiou A., Mitra D., Gupta Y., 2008, MNRAS, 388, 261
Karastergiou A., 2009, MNRAS, 392, L60
Karastergiou A., Johnston S., 2004, MNRAS, 352, 689
Karastergiou A., Johnston S., 2006, MNRAS, 365, 353
Karastergiou A., Johnston S., 2007, MNRAS, 380, 1678
Karastergiou A., Johnston S., Manchester R. N., 2005, MNRAS, 359, 481
Keith M. J. et al., 2010, MNRAS, 409, 619
Keith M. J. et al., 2012, MNRAS, 419, 1752
Kramer M. et al., 2003, MNRAS, 342, 1299
Li X. H., Han J. L., 2003, A&A, 410, 253

Lorimer D. R., Kramer M., 2005, Handbook of Pulsar Astronomy. Cambridge Univ. Press, Cambridge
Lyne A. G., Manchester R. N., 1988, MNRAS, 234, 477
Lyne A. G., Smith F. G., 1989, MNRAS, 237, 533
McKinnon M. M., Stinebring D. R., 2000, ApJ, 529, 435
Manchester R. N., 1972, ApJ, 172, 43
Manchester R. N., Taylor J. H., 1977, Pulsars. Freeman, San Francisco
Naghizadeh-Khouei J., Clarke D., 1993, A&A, 274, 968
Noutsos A., Johnston S., Kramer M., Karastergiou A., 2008, MNRAS, 386, 1881
Noutsos A., Karastergiou A., Kramer M., Johnston S., Stappers B. W., 2009, MNRAS, 396, 1559
Radhakrishnan V., Cooke D. J., 1969, Astrophys. Lett., 3, 225
Radhakrishnan V., Rankin J. M., 1990, ApJ, 352, 258
Ramachandran R., Backer D. C., Rankin J. M., Weisberg J. M., Devine K. E., 2004, ApJ, 606, 1167
Rankin J. M., 1983, ApJ, 274, 333
Rankin J. M., 1993, ApJ, 405, 285
Simmons J. F. L., Stewart B. G., 1985, A&A, 142, 100
Sofue Y., Fujimoto M., 1983, ApJ, 265, 722
Stairs I. H., Thorsett S. E., Camilo F., 1999, ApJS, 123, 627
Stinebring D. R., Cordes J. M., Rankin J. M., Weisberg J. M., Boriakoff V., 1984, ApJS, 55, 247
Taylor J. H., Cordes J. M., 1993, ApJ, 411, 674
Thomson R. C., Nelson A. H., 1980, MNRAS, 191, 863
Vallée J. P., 2005, ApJ, 619, 297
van Straten W., 2004, ApJS, 152, 129
von Hoensbroech A., Xilouris K. M., 1997, A&A, 324, 981
von Hoensbroech A., Lesch H., Kunzl T., 1998, A&A, 336, 209
Wardle J., Kronberg P., 1974, ApJ, 194, 249
Weisberg J. M., Cordes J. M., Kuan B., Devine K. E., Green J. T., Backer D. C., 2004, ApJS, 150, 317
Weltevrede P., Johnston S., 2008, MNRAS, 391, 1210
Xilouris K. M., Kramer M., Jessner A., von Hoensbroech A., Lorimer D., Wielebinski R., Wolszczan A., Camilo F., 1998, ApJ, 501, 286
Yan W. M. et al., 2011, MNRAS, 414, 2087

This paper has been typeset from a TEX/LATEX file prepared by the author.